Published in final edited form as:
Biofabrication. ; 7(1): 015006. doi:10.1088/1758-5090/7/1/015006.

Metal ion-assisted self-assembly of complexes for controlled and sustained release of minocycline for biomedical applications

Zhiling Zhang[1], **Zhicheng Wang**[1], **Jia Nong**[1], **Camilla A. Nix**[1], **Hai-Feng Ji**[2], and **Yinghui Zhong**[1,*]

[1]School of Biomedical Engineering, Science and Health Systems, Drexel University, 3141 Chestnut Street, Philadelphia, PA 19104, USA

[2]Department of Chemistry, Drexel University, 3141 Chestnut Street, Philadelphia, PA 19104, USA

Abstract

This study reports the development of novel drug delivery complexes self-assembled by divalent metal ion-assisted coacervation for controlled and sustained release of a hydrophilic small drug molecule minocycline (MH). MH is a multifaceted agent that has demonstrated therapeutic effects in infection, inflammation, tumor, as well as cardiovascular, renal, and neurological disorders due to its anti-microbial, anti-inflammatory, and cytoprotective properties. However, the inability to translate the high doses used in experimental animals to tolerable doses in human patients limits its clinical application. Localized delivery can potentially expose the diseased tissue to high concentrations of MH that systemic delivery cannot achieve, while minimizing the side effects from systemic exposure. The strong metal ion binding-assisted interaction enabled high drug entrapment and loading efficiency, and stable long term release for more than 71 days. Released MH demonstrated potent anti-biofilm, anti-inflammatory, and neuroprotective activities. Furthermore, MH release from the complexes is pH-sensitive as the chelation between minocycline and metal ions decreases with pH, allowing ‘smart’ drug release in response to the severity of pathology-induced tissue acidosis. This novel metal ion binding-mediated drug delivery mechanism can potentially be applied to other drugs that have high binding affinity for metal ions and may lead to the development of new delivery systems for a variety of drugs.

Keywords

controlled release; complex; minocycline; drug delivery; metal ion

1. Introduction

Minocycline Hydrochloride (MH) is a tetracycline derivative antibiotic that also has anti-inflammatory, anti-oxidative, and anti-apoptotic properties [1]. It is commonly used clinically to treat infection and inflammation [1–4]. In addition, studies have shown that by

*Correspondence and requests for materials should be addressed to: Yinghui Zhong, Ph.D., Drexel University, 3141 Chestnut Street, Philadelphia, PA 19104, yz348@drexel.edu, Phone: 215-895-1559, Fax: 215-895-4983.

attenuating the expression of matrix metalloproteases, MH could inhibit smooth muscle cell proliferation and neointimal hyperplasia after arterial injury [5], and reduce tumor expansion and migration [6]. MH also demonstrated cytoprotective properties in the cardiovascular, renal, and central nervous systems [7]. It has been shown to protect cardiac myocytes against ischemia-reperfusion injury and ameliorate cardiac dysfunction and cell loss [8, 9], reduce cell apoptosis and inflammation in ischemic renal diseases [10], and exert neuroprotective effects in various neurological disorders including stroke [11], spinal cord injury [12], Parkinson's disease [13], multiple sclerosis [14], Amyotrophic lateral sclerosis (ALS) [15] and Alzheimer's disease [16].

Many of these diseases require continuous and high concentrations of MH treatment at dose levels much higher than the standard human dose of 3 mg/kg [17]. For example, to inhibit tumor growth in mice, systemic administration of 60–120 mg/kg MH was required for 4 weeks [18]; to reduce neointima formation after artery injury, animals need to receive intraperitoneal injections of 70–100 mg/kg MH for 16 days [5]; to reduce neuronal death and improve functional outcome in animal models of multiple sclerosis and Parkinson's disease, 3–4 weeks of MH treatment at a dose of 45 mg/kg was required [13, 19]. However, systemic administration of high doses of MH for extended period of time has been shown to cause morbidity, liver toxicity and even death in experimental animals [5, 12]. Thus, localized delivery of MH can potentially expose the diseased tissue to high concentrations of MH while minimizing the deleterious side effects from systemic exposure. However, current drug delivery systems are not ideal for local delivery of bioactive MH for an extended period of time. MH is a small molecule drug (MW 494 Da) with high water solubility. Therefore it is released very quickly (less than 24 h) from hydrophilic drug delivery systems [20–22]. Furthermore, while hydrophobic poly(lactic-co-glycolic acid) (PLGA) microspheres [2, 23] or nanoparticles [24] have been used as drug carriers for MH encapsulation and release, the acidic degradation products of PLGA can reduce local tissue pH and subsequently elicit host inflammation [25, 26]. In addition, MH diffuses into the aqueous phase easily due to its high water solubility, leading to low loading efficiency (up to 1.92%) of MH in the PLGA particles [24].

In this study we developed novel MH-encapsulated complexes based on metal ion binding-mediated interaction for sustained local delivery of bioactive MH. MH can chelate multivalent metal ions such as Ca^{2+} and Mg^{2+} to form positively charged chelates without affecting its biological activities [27]. Dextran sulfate (DS), a biocompatible polysaccharide, also has high binding affinity for divalent metal ions such as Ca^{2+} and Mg^{2+} ions [28]. Our lab has previously discovered that Ca^{2+} ions could be used as linkers to attach MH to DS in a layer-by-layer fashion [29]. Utilizing this property, we developed an electrostatic layer-by-layer thin film coating using DS+Ca^{2+}, MH, and gelatin type A as building blocks. While the coating can be used on implanted medical devices for local delivery of MH, they are not readily used in applications where implanted devices are not involved. In the present study, we discovered that DS and MH can form insoluble complex in the presence of Ca^{2+} or Mg^{2+}. It is noteworthy that unlike conventional coacervation where two oppositely charged polymers are required to form the complex [30], in our system only one charged polymer (DS) is required for complex formation. MH is electrically neutral in the pH range of complex formation (5.5–6.5). This is the first time that metal ion binding-assisted interaction

is used to induce insoluble complex formation between a charged polymer and a neutral small drug molecule, which enables high drug entrapment efficiency (more than 96.9%), high drug loading efficiency (around 45%), and stable long term release for more than 71 days. In this study, we investigated the parameters that control MH loading and release, and examined the pH-sensitive release behavior of MH from the complexes. Further, the bioactivity of released MH including antibacterial, anti-inflammatory, and neuroprotective potencies was assessed. This novel drug delivery system is highly promising for long-term local delivery of MH for a variety of clinical applications.

2. Materials and methods

2.1 Materials

All the chemicals, unless otherwise specified, were obtained from Sigma-Aldrich and used without further purification. *Escherichia coli* (ATCC 25922) and *Staphylococcus aureus* (ATCC 25923) strains were purchased from American Type Culture Collection (ATCC, Manassas, VA). A multi-drug resistant *Acinetobacter baumannii* clinical isolate was locally isolated from a hospitalized patient having invasive infection following a protocol approved by the Institutional Review Board of Drexel University.

2.2 Preparation of MH-metal ion-DS complex

Dextran sulfate (500 kDa) was dissolved in $CaCl_2$ or $MgCl_2$ solution at different concentrations to study the effect of metal ion concentration on MH loading and release. Minocycline solution (2 mg/ml) was prepared in deionized (DI) water. 150 μl DS solution was mixed with equal volume of MH solution and vortexed for 10 sec to induce complex formation. The complex was collected by centrifugation at 10,000 rpm for 10 min and washed three times with DI water.

2.3 Fourier-transform infrared (FTIR) spectroscopy, Zeta potential measurement, and scanning electron microscopy (SEM)

1.2 mg/ml DS, 1 mg/ml MH, and 7.2 mM $CaCl_2$ or $MgCl_2$ were used for complex formation. Complexes containing 100 μg MH were rinsed with DI water for 3 times to remove unbound metal ions. For FTIR spectroscopy measurement, DS, MH, and the complexes were lyophilized and characterized using a Perkin-Elmer Spectrum One Fourier transform IR absorption spectrophotometer (Waltham, MA, USA). For zeta potential measurement the complexes were re-suspended in 1 ml DI water after washing and analyzed using a Malvern Nano ZS90 zeta-sizer (Westborough, MA, USA).

For SEM sample preparation, 10 μl complex suspension was spread on a silicon wafer and lyophilized. The silicon wafer was mounted on an aluminum stub, sputtered with 10 nm Pt-Pd and viewed with a Zeiss Supra 50VP SEM at an operating voltage of 5 kV.

2.4 Entrapment efficiency and loading efficiency

The amount of MH and DS loaded in the complex was determined by subtracting the amount of MH and DS remaining in the supernatant from the initial amount of MH and DS added in the solution for complex formation. The concentration of MH in the supernatant

was measured by UV-vis spectroscopy at 245 nm (DS have negligible absorbance at this wavelength). DS concentration in the supernatant was determined by titration of sulfate groups with the cationic dye toluidine blue [31]. The entrapment efficiency of MH in the DS-MH complexes was calculated as the ratio of the weight of MH encapsulated in the complex to the total weight of MH added in the solution. The loading efficiency of MH in the DS-MH complexes was calculated as the ratio of the weight of MH encapsulated in the complex to the total weight of the complex.

2.5 Quantification of MH release

The complexes encapsulating 300 μg MH were incubated at 37° C in 300 μl of Hank's Balanced Salt Solution (HBSS) for quantification of MH release. The release medium was changed every 24 h till drug release was completed. The amount of MH released every 24 h was determined by UV absorbance at 245nm. For quantification of MH release in HBSS supplemented with bovine serum albumin (BSA), the amount of released MH was determined by UV absorbance at 380nm (DS and BSA have negligible absorbance at this wavelength).

2.6 Anti-inflammatory bioactivity of released MH

RAW264.7 murine macrophages (kindly provided by Dr. Narayan Avadhani, University of Pennsylvania) were cultured in Dulbecco's modified Eagle's medium (DMEM) supplemented with 10% fetal bovine serum (FBS) and 1% penicillin/streptomycin. The cells were seeded in 96-well tissue culture plates at a density of 60,000 cells per well. 24 h after seeding, the cells were stimulated with 400 pg/ml lipopolysaccharide (LPS), a potent proinflammatory endotoxin, and treated with MH that was released during a 24 h period and diluted to 0.5 μg/ml, or 0.5 μg/ml fresh MH. After 48 h, the accumulated levels of nitrite in the cell culture medium, as an indication of NO, was measured with Griess reagent (Promega).

2.7 Biofilm assay

Tryptone Soya Broth (TSB) medium was used as the release medium for biofilm assay. Bacterial suspensions were inoculated in 96-well plates at a density of 2×10^4 cells per well, and incubated with 40 μg/ml fresh MH or MH released in the first day from the DS-MH complexes (diluted to 40 μg/ml). The biofilms were allowed to set by incubating at 37°C in a stationary incubator for 24 h. For quantification of bacterial viability, the wells were washed three times with sterile PBS to remove loose planktonic cells, and incubated with 200 μl of XTT reagent in the dark at 37°C for 2 h. The metabolic conversion of XTT into orange-coloured product was measured photometrically at 492 nm using a microtiter plate reader (BioTek). Only surviving/live bacterial cells show evidence of respiration and metabolize XTT reagent to reduce it to an orange coloured soluble product [32]. For visualization of live and dead bacteria, the cells were stained with LIVE/DEAD BacLight Bacterial Viability kit (Invitrogen), and examined by EVOS FL Color Imaging System (AMG).

2.8 Neuroprotection by released MH

Rat cortical neurons were isolated from E17 rat embryos in accordance with protocols approved by Drexel University's IACUC committee. The cortices were dissected, minced, and enzymatically dissociated with 0.25% trypsin and 1mM EDTA for 2 min at 37°C. Then the tissue was triturated through a fire polished glass pipette in 5100 U/ml DNase in HBSS solution to obtain dissociated cells. Following centrifugation, the cells were re-suspended in neurobasal medium (Invitrogen) supplemented with 2% B27 Supplement (Invitrogen) and 2mM L-glutamine, and seeded in 48-well culture plates at a density of 120,000 cells/cm^2. After 7 days of culture, the culture medium was replaced with neurobasal medium supplemented with B27 minus antioxidants (AO) to remove the neuroprotective anti-oxidants. After 6 h the neurons were treated with 100 μM hydrogen peroxide (H_2O_2), 15 μg/ml fresh MH, or MH that was released during a 24 h period on day 1 from Ca^{2+}- or Mg^{2+}-complex (diluted to 15 μg/ml) for 24 h. Cell viability was determined using cell counting kit-8 (CCK-8, Dojindo). Finally, the cells were stained with live/dead staining (Calcein AM for live cells and ethidium homodimer for dead cells) to visualize neuron morphology and survival. Fluorescent images were captured using an inverted fluorescence microscope (Leica).

2.9 Statistical analysis

Multiple pairwise comparisons were conducted using a general linear analysis of variance (ANOVA) model and Tukey test. $P < 0.05$ was considered statistically significant. Data are presented as mean ± standard deviations.

3. Results and discussions

3.1 Formation of DS-metal ion-MH complex

The self-assembly of insoluble DS-MH complex occurred upon mixing MH and DS solutions in the presence of Ca^{2+} or Mg^{2+} ions (figure 1). No insoluble complex was formed when any two of the three components (DS, MH, and metal ions) were mixed. MH is a yellow compound. MH in DI water, $CaC1_2$, or $MgCl_2$ solution remains yellow colour. When MH, DS, and metal ions were mixed together, the Ca^{2+}-based complex showed the same yellow colour as MH, while the Mg^{2+}-based complex had a light yellow colour. The cause for the change of colour in Mg^{2+}-based complex is unclear. MH loading in both complexes is similar (as discussed later), suggesting that the change in colour is not due to different MH loading. Bioactivity assay showed that the colour change didn't affect the bioactivity of released MH.

The DS-MH complex suspension was collected by centrifugation. FTIR spectra (figure 2(*A*)) revealed that DS had an adsorption peak at 1233 cm^{-1} (asymmetric stretching of S=O in sulfate group) [33], which was shifted to 1219 cm^{-1} in the Ca^{2+}-based complex and 1224 cm^{-1} in the Mg^{2+}-based complex, respectively (figure 2(*C*) and (*D*)). Furthermore, DS had a peak at 3479 cm^{-1} originating from OH group, and it was shifted to 3403 cm^{-1} in the Ca^{2+}-based complex and 3428 cm^{-1} in Mg^{2+}-based complex, respectively. These results suggest that the sulfate and hydroxyl groups in the DS molecules interact with MH or metal ions in the complex. figure 2(*B*) shows that MH had a peak at 1583 cm^{-1}, corresponding to C=O

stretching on C_{11} [34], which is part of a chelating site (C_{10}-C_{11}-C_{12}) for Ca^{2+} or Mg^{2+} ions (Scheme 1B) [35]. When forming complex with DS and metal ions, this peak was shifted to 1607 cm^{-1} in the Ca^{2+}-based complex and 1606 cm^{-1} in the Mg^{2+}-based complex, respectively. In conclusion, FTIR spectra clearly demonstrated the interaction of DS with MH and metal ions.

The sulfate groups in DS have a high binding affinity for divalent metal ions including Ca^{2+} or Mg^{2+} [36]. Our previously study has shown that MH could chelate both free metal ions and metal ions that are attached to the sulfate groups in DS [29]. Thus, DS could interact with MH through metal ion binding (Scheme 1C). One MH molecule has two metal ion binding sites as shown in Scheme 1B (red boxes). However, although only the functional group on C_{10}-C_{11}-C_{12} could be detected in the complexes by FTIR, we cannot rule out the possibility that the other metal ion binding site also participates in complex formation. MH has four p*K*a values, 5 and 9.5 for the two amine functional groups on C7 and C4, respectively, and 2.8 and 7.8 for the two hydroxyl groups at C3 and C4, respectively [37]. Thus, It is zwitterionic at the pH of complex formation (5.5–6.5) with one negatively charge from deprotonation of the hydroxyl group at C3 (pKa = 2.8) and one positive charge from the ammonium group at C4 (pKa = 9.5) [38]. The positively charged ammonium group at C4 in MH could form electrostatic interaction with the negatively charged sulfate group in DS (Scheme 1C). Furthermore, the hydroxyl group in DS can potentially form hydrogen bonding with the hydroxyl, carbonyl and amide groups in MH (Scheme 1B, green boxes). Although MH could potentially interact with DS through electrostatic interaction and hydrogen bonding, no insoluble complex was formed when DS and MH were mixed together in the absence of metal ions. Similarly, mixing DS and metal ions together without MH did not lead to formation of insoluble complex either even though DS is known to have high binding affinity for Ca^{2+} and Mg^{2+} ions.[28] We speculate that for insoluble complex formation the crosslinking of DS is needed, which can only be achieved by interacting with both metal ions and MH since all three components are necessary for insoluble complex formation. We postulate that one MH molecule can interact with at least two functional groups in DS simultaneously through metal ion binding, electrostatic interaction, or hydrogen bonding to induce intra and intermolecular crosslinking of DS (Scheme 1C), and at least one of these interactions must be metal ion binding since electrostatic interaction and hydrogen bonding are insufficient to induce insoluble complex formation between DS and MH.

Zeta potential measurement (figure 3(*A*)) shows that the complexes remained negatively charged over a wide range of DS/MH mass ratio from 0.3 to 1.8. Little complex was formed below the ratio of 0.3, and the entrapment efficiencies for both MH and DS reached peak at the ratio of 1.2 (figure 4(*B*) and (*D*)), after which MH loading reached plateau. Thus, within the ratio range of effective complex formation the complex remained negatively charged.

Scanning electron microscopy (SEM) images (figure 3(*B*) and (*C*)) show that the complexes were composed of aggregated nanoparticles with size ranging from 50 to 100 nm. These complexes can be embedded in various carriers such as wound dressing, implant or implant coatings, or hydrogels for local delivery of MH depending on specific biomedical applications. For example, studies have shown that intrathecal injection of drug-loaded

hydrogel can bypass the diffusive barrier presented by the pia mater and has been shown to be safe and effective to deliver drugs to the spinal cord tissue [39–42]. Our laboratory is investigating using injectable hydrogel loaded with MH-containing complexes for local delivery of MH to provide neruoprotection for spinal cord repair.

We investigated the effects of metal ion concentration and DS/MH mass ratio on the encapsulation efficiency. As shown in figure 4(*A*), for Ca^{2+}-based complex the encapsulation efficiencies for both MH and DS increased rapidly with increasing Ca^{2+} concentration till 3.6 mM (94.7 ± 0.7% and 94.4 ± 0.6%), after which further increasing Ca^{2+} concentration to 7.2 mM only slightly increased the encapsulation efficiencies of MH and DS to 96.9 ± 0.2% and 97.8 ± 0.1%, respectively. Figure 4(*C*) demonstrates that for Mg^{2+}-based complex the encapsulation efficiencies of MH and DS versus Mg^{2+} concentration showed a similar pattern, except that they reached plateau (98.5 ± 0.2% and 99.4 ± 0.3%) at 5.4 mM. Further increasing Mg^{2+} concentration to 7.2 mM had little effect on the encapsulation efficiencies of MH and DS (98.0 ± 0.4% and 99.4 ± 0.1%). It is likely that increasing metal ion concentration at the beginning allowed more metal ions to bind to DS molecules which subsequently increased MH loading through metal ion binding. When metal ion binding reached saturation, then further increasing metal ion concentration couldn't increase MH loading in the complex anymore. This result supports our hypothesis that divalent metal ions play an important role in DS and MH encapsulation into the complex. When the encapsulation efficiencies of MH and DS versus metal ion concentration reached plateau, the loading efficiency of MH reached plateau as well. When the concentration of metal ions was 7.2 mM, Ca^{2+}-based complex and Mg^{2+}-based complex had similar loading efficiency of MH (45.3% and 45.2%).

The encapsulation efficiency is also affected by the mass ratio of DS to MH. In this study the concentration of MH was kept at 1 mg/ml. As shown in figure 4(*B*), at a low DS/MH ratio of 0.1–0.3 the encapsulation efficiency of MH in Ca^{2+}-based complexes was relatively low. It increased rapidly with increasing DS/MH ratio and reached plateau (96.9 ± 0.2%) at the ratio of 1.2. This result suggests that when the ratio was below 1.2 there was excess MH in the solution. In contrast, the encapsulation efficiency of DS was high (96.0 ± 1.0%) even at the low DS/MH ratio of 0.1, and it only increased slightly when further increasing the DS/MH ratio and reached peak (97.5 ± 0.1%) at the ratio of 1.2, after which the encapsulation efficiency started to decrease. This result suggests that DS became excessive when the ratio was above 1.2. The encapsulation efficiencies of MH and DS versus DS/MH ratio for Mg^{2+}-based complex showed similar pattern (figure 4(*D*)) and also reached peak (98.0 ± 0.4% and 99.4 ± 0.1%) at the ratio of 1.2. Collectively, these results demonstrate that 1.2 is the optimum DS/MH ratio for complex formation.

3.2 Effect of metal ion concentration on MH release from DS-metal ion-MH complex

Since metal ions are essential for complex formation, it is possible that metal ions play an important role in mediating MH release from the complexes. Different concentrations of metal ions were used for complex formation to investigate the effect of metal ion concentration on MH release. The binding of MH or DS to metal ions is reversible. Thus, MH release from the complex could be mediated by detachment of MH-metal ion chelates

from DS, or dissociation of MH from DS-bound metal ions. We have demonstrated from figure 4(*A*) that the encapsulation efficiency of MH in Ca^{2+}-based complex was increased from 52.0 ± 7.9% to 94.7 ± 0.7% when increasing Ca^{2+} concentration from 1.8 to 3.6 mM, suggesting that more Ca^{2+} ions were incorporated into the system. Consistent with this result, MH release in HBSS was prolonged from 40 to 54 days (figure 5(*A*) and (*B*), black line). For Mg^{2+}-based complex, the encapsulation efficiency was increased from 89.8 ± 1.0% to 99.4 ± 0.1% when increasing Mg^{2+} concentration from 3.6 to 7.2 mM. Likewise, MH release was prolonged from 41 to 71 days (figure 5(*C*) and (*D*), black line). For all the conditions, MH release followed near zero-order release kinetics after a small initial burst. Higher concentration of metal ions decreased the initial burst and prolonged the duration of release.

In the body the complex might be exposed to various types of body fluids which contain proteins. For example, when using balloon angioplasty and stenting to open the narrowed arteries the complexes could be embedded in the stent to prevent smooth muscle cell proliferation and restenosis. Under this circumstance, the complex will be exposed to blood proteins. The complex can also be embedded in hydrogel and injected into the intrathecal space between the dura mater and spinal cord tissue to promote spinal cord repair. In this case, the complexes will be exposed to cerebrospinal fluid (CSF). To study whether proteins in body fluids will interact with the complexes and alter the release profile, we added BSA in HBSS release media to more closely mimic the human body condition. Albumin was chosen because it is the most abundant protein in most body fluids. HBSS containing 0.175 and 40 mg/ml BSA was used to mimic CSF and blood, respectively [43, 44]. Figure 5 shows that both concentrations of BSA in the release media had little effect on MH release from Ca^{2+}- or Mg^{2+}-based complex, suggesting that stable MH release could be still maintained in the in vivo environment.

3.3 Effect of pH on MH release from DS-metal ion-MH complex

Acidic pH is commonly found under pathological conditions such as injury, injection, inflammation, and tumor [45–48]. To simulate pathological and physiological conditions, release study was performed in HBSS at pH 6.0 and 7.4. As shown in figure 6(*A*) and (*B*), when the metal ion concentration used in complex formation was 7.2 mM, MH release from Ca^{2+}- and Mg^{2+}-based complexes lasted 22 and 24 days at pH 6.0, versus 55 and 71 days of stable release at physiological pH of 7.4. Studies have shown that the binding affinity of tetracycline to divalent metal ions decreases with pH [49]. Thus, reduced pH can weaken the chelation between MH and metal ions in the complex and facilitate MH release. The pH-sensitive release behavior further supports the hypothesis that reversible metal ion binding play an important role in mediating MH release from the complexes. Thus, the DS-metal ion-MH complex could be used as a “smart” drug delivery system to actively deliver MH in response to the severity of pathology-induced tissue acidosis.

3.4 Anti-inflammatory activity of released MH

The anti-inflammatory activity of released MH was examined using the well-established macrophage cell line RAW264.7. The macrophages were stimulated with LPS for upregulating the production of nitric oxide (NO), a cytotoxic molecule generated by

macrophages in response to infection and inflammation [50]. MH as a potent anti-inflammatory drug has been shown to be able to inhibit the activation of macrophages and NO production [51]. MH released during a 24 h period on the last day of release from Ca^{2+}- or Mg^{2+}-based complex was diluted to 0.5 μg/ml and added to LPS-treated macrophage cultures. The NO level in these cultures was compared to that in the culture treated with 0.5 μg/ml freshly prepared MH. As shown in figure 7, MH released from either complex significantly inhibited NO production by LPS-stimulated macrophages to the same degree as fresh MH, suggesting that released MH retained the same bioactivity as fresh MH even after 55 (from Ca^{2+}-based complex) or 71 (from Mg^{2+}-based complex) days of release. This result indicates that this drug delivery system not only maintained the bioactivity of MH, but also released physiologically relevant amount of MH throughout the duration of release. MH degrades rapidly in aqueous solution, especially at body temperature [22]. A number of studies have shown that Ca^{2+} enhances the stability of MH by forming more stable Ca^{2+}-MH chelates [22, 52].Our study demonstrated that both Ca^{2+} and Mg^{2+} helped to preserve the bioactivity of MH. Thus, the MH-releasing complexes hold great promise for the treatment of chronic inflammation.

3.5 Antibacterial potency of released MH

Medical implants are susceptible for bacteria adhesion and subsequent biofilm formation [53–56]. Conventional systemic antibiotic therapy and the body's natural defense system are usually ineffective in killing bacteria within a biofilm [54, 56]. Following implantation the first 6 hours have been identified as a "decisive period" during which inhibition of bacterial adhesion is critical for the long-term success of an implant [54, 55]. The complex can potentially be embedded into polymer-based implants or implant coatings for local release of MH to inhibit biofilm formation during the "decisive period". To evaluate the antibacterial and anti-biofilm efficacies of the complexes, we selected three common bacterial species that are known to be involved in infection and biofilm formation, including *A. baumannii*, a strong biofilm producer that is multidrug resistant and difficult to control and treat in the healthcare setting [57]. Figure 8(*A*) shows that for untreated controls all three bacterial species formed biofilm after one day of incubation, whereas only a few bacteria were present when the cells were treated with either fresh MH, or MH released from Ca^{2+}- or Mg^{2+}-based complexes. XTT quantification (figure 8(*B*)) confirmed that fresh or released MH significantly inhibited biofilm formation by all three virulent pathogens, leaving negligible pathogens on the substrates. The body's defense system can easily clear the few surviving bacteria since no biofilm is formed [53]. The bacteria number in the fresh MH-treated group was not significantly different from that in the released MH-treated groups.

3.6 Neuroprotection by released MH

Rat cortical neurons were treated with H_2O_2, one of the cytotoxic reactive oxygen species that induce oxidative stress and neuronal death in neurotrauma and neurodegenerative diseases [58–60]. Figure 9(*A*)–(*E*) shows that 100 μM H_2O_2 killed most neurons, while 15 μg/ml fresh MH and MH released from both Ca^{2+} and Mg^{2+}-based complexes substantially improved neuron survival. Quantitative cell counting assay (figure 9(*F*)) confirmed that both fresh MH and released MH significantly inhibited H_2O_2-induced neurotoxicity, and the cell viability in cultures treated with MH released from either Ca^{2+}- or Mg^{2+}-based complex was

not significantly different from that in cultures treated with fresh MH. As an antioxidant and anti-apoptotic agent, MH has demonstrated potent neuroprotective effects in neurotrauma and neurological disorders at high concentrations (15–75 μg/ml) [61–63]. However, systemic administration of MH at a high dose level of 50 mg/kg only results in 0.5 μg/ml MH in the cerebrospinal fluid (CSF) [14]. While this concentration is sufficient for anti-inflammatory effect, it is far below the neuroprotective level. Thus, local delivery of MH from the complex can potentially expose the injured neural tissue to high concentrations of MH while avoiding the deleterious side effects from systemic exposure. For applications where most neuronal loss happens in the acute stage (within 24 hr), such as traumatic brain injury [47], spinal cord injury [64, 65], and stroke [66], initial burst release of high-dose MH from the complexes can provide neuroprotection, and subsequent slow release of MH can target chronic inflammation following neural injury. For neurodegenerative diseases such as Alzheimer's disease and Parkinson's disease which are closely associated with chronic neuroinflammation [67], sustained local delivery of MH can potentially inhibit the progression of these debilitating diseases while obviating the side effects from long term systemic exposure. Thus, this novel drug delivery system is highly promising to be used for neural repair.

4. Conclusions

This study investigates novel drug delivery complexes self-assembled by divalent metal ion-assisted coacervation of MH and DS for controlled and sustained release of MH, a hydrophilic small molecule drug. This is the first time that metal ion binding is used for complex coacervation between a charged polymer and a neutral small drug molecule. We have demonstrated that the loading and release of MH can be regulated by tailoring the binding affinity between MH and DS through varying metal ion concentration. Furthermore, MH release from the complexes is pH-sensitive as the strength of chelation between MH and metal ions decreases with pH, allowing 'smart' drug release in response to the severity of pathology-induced tissue acidosis. The released MH remained bioactive throughout the duration of release because metal ions enhance the stability of minocycline by forming more stable chelates. Released MH demonstrated potent anti-biofilm, anti-inflammatory, and neuroprotective activities. The novel complex allows local delivery of high concentrations of MH that systemic delivery cannot achieve for effective treatment while avoiding the deleterious side effects from systemic exposure. Collectively, this drug delivery system has great potential to be used in a variety of clinical applications including infection, inflammation, tumor, as well as cardiovascular, renal and neural protection. Furthermore, this novel metal ion binding-mediated complex coacervation and drug delivery mechanism can potentially be employed to deliver other drugs that have a high metal ion binding affinity, and may lead to the development of new delivery vehicles for a variety of drugs.

Acknowlegements

We thank Dr. Narayan Avadhani (Department of Animal Biology, University of Pennsylvania) for kindly providing RAW264.7 macrophages, and Dr. Suresh G. Joshi (Department of Surgery and Department of Microbiology and Immunology, Drexel University College of Medicine) for his technical support with the anti-biofilm study. This research was supported by the National Institute of Neurological Disorders And Stroke of the National Institutes of Health under Award Number R21NS084379.

References

1. Garrido-Mesa N, Zarzuelo A, Galvez J. Minocycline: far beyond an antibiotic. Br. J. Pharmacol. 2013; 169:337–352. [PubMed: 23441623]
2. Vandekerckhove B NA, Quirynen M, van Steenberghe D. The use of locally-delivered minocycline in the treatment of chronic periodontitis. A review of the literature. J. Clin. Periodontol. 1998; 25:964–968. [PubMed: 9839854]
3. Humbert P, Treffel P, Chapuis J-F, Buchet S, Derancourt C, Agache P. The tetracyclines in dermatology. J. Am. Acad. Dermatol. 1991; 25:691–697. [PubMed: 1791227]
4. Kloppenburg M, Breedveld FC, Terwiel JP, Mallee C, Dijkmans BA. Minocycline in active rheumatoid arthritis. A double-blind, placebo-controlled trial Arthritis Rheum. 1994; 37:629–636.
5. Pinney SP, Chen HJ, Liang D, Wang X, Schwartz A, Rabbani LE. Minocycline inhibits smooth muscle cell proliferation, migration and neointima formation after arterial injury. J. Cardiovasc. Pharmacol. 2003; 42:469–476. [PubMed: 14508231]
6. Markovic DS, Vinnakota K, van Rooijen N, Kiwit J, Synowitz M, Glass R, Kettenmann H. Minocycline reduces glioma expansion and invasion by attenuating microglial MT1-MMP expression. Brain. Behav. Immun. 2011; 25:624–628. [PubMed: 21324352]
7. Jordan J, Fernandez-Gomez FJ, Ramos M, Ikuta I, Aguirre N, Galindo MF. Minocycline and cytoprotection: shedding new light on a shadowy controversy. Curr. Drug Delivery. 2007; 4:225–231.
8. Scarabelli TM, et al. Minocycline inhibits caspase activation and reactivation, increases the ratio of XIAP to smac/DIABLO, and reduces the mitochondrial leakage of cytochrome C and smac/DIABLO. J. Am. Coll. Cardiol. 2004; 43:865–874. [PubMed: 14998631]
9. Tao R, Kim SH, Honbo N, Karliner JS, Alano CC. Minocycline protects cardiac myocytes against simulated ischemia-reperfusion injury by inhibiting poly(ADP-ribose) polymerase-1. J. Cardiovasc. Pharmacol. 2010; 56:659–668. [PubMed: 20881608]
10. Kelly K, Sutton T, Weathered N, Ray N, Caldwell E, Plotkin Z, Dagher P. Minocycline inhibits apoptosis and inflammation in a rat model of ischemic renal injury. Am. J. Physiol.: Renal, Fluid Electrolyte Physiol. 2004; 287:F760–F766. [PubMed: 15172883]
11. Fagan SC, Cronic LE, Hess DC. Minocycline Development for Acute Ischemic Stroke. Transl. Stroke Res. 2011; 2:202–208. [PubMed: 21909339]
12. Lee SM, Yune TY, Kim SJ, Park DW, Lee YK, Kim YC, Oh YJ, Markelonis GJ, Oh TH. Minocycline reduces cell death and improves functional recovery after traumatic spinal cord injury in the rat. J. Neurotrauma. 2003; 20:1017–1027. [PubMed: 14588118]
13. Quintero EM, Willis L, Singleton R, Harris N, Huang P, Bhat N, Granholm AC. Behavioral and morphological effects of minocycline in the 6-hydroxydopamine rat model of Parkinson's disease. Brain Res. 2006; 1093:198–207. [PubMed: 16712819]
14. Maier K, Merkler D, Gerber J, Taheri N, Kuhnert AV, Williams SK, Neusch C, Bahr M, Diem R. Multiple neuroprotective mechanisms of minocycline in autoimmune CNS inflammation. Neurobiol Dis. 2007; 25:514–525. [PubMed: 17239606]
15. Zhu S, et al. Minocycline inhibits cytochrome c release and delays progression of amyotrophic lateral sclerosis in mice. Nature. 2002; 417:74–78. [PubMed: 11986668]
16. Choi Y, et al. Minocycline attenuates neuronal cell death and improves cognitive impairment in Alzheimer's disease models. Neuropsychopharmacology. 2007; 32:2393–2404. [PubMed: 17406652]
17. Xu L, Fagan SC, Waller JL, Edwards D, Borlongan CV, Zheng J, Hill WD, Feuerstein G, Hess DC. Low dose intravenous minocycline is neuroprotective after middle cerebral artery occlusion-reperfusion in rats. BMC Neurol. 2004; 4:7. [PubMed: 15109399]
18. Pourgholami MH, Ataie-Kachoie P, Badar S, Morris DL. Minocycline inhibits malignant ascites of ovarian cancer through targeting multiple signaling pathways. Gynecol. Oncol. 2013; 129:113–119. [PubMed: 23274564]
19. Maier K, Merkler D, Gerber J, Taheri N, Kuhnert AV, Williams SK, Neusch C, Bahr M, Diem R. Multiple neuroprotective mechanisms of minocycline in autoimmune CNS inflammation. Neurobiol. Dis. 2007; 25:514–525. [PubMed: 17239606]

20. Jones DS, Lorimer CP, McCoy CP, Gorman SP. Characterization of the physicochemical, antimicrobial, and drug release properties of thermoresponsive hydrogel copolymers designed for medical device applications. J. Biomed. Mater. Res. B. 2008; 85:417–426.
21. Sung JH, et al. Gel characterisation and in vivo evaluation of minocycline-loaded wound dressing with enhanced wound healing using polyvinyl alcohol and chitosan. Int. J. Pharm. 2010; 392:232–240. [PubMed: 20230884]
22. Soliman GM, Choi AO, Maysinger D, Winnik FM. Minocycline Block Copolymer Micelles and their Anti-Inflammatory Effects on Microglia. Macromol. Biosci. 2010; 10:278–288. [PubMed: 19937662]
23. Williams RC, Paquette DW, Offenbacher S, Adams DF, Armitage GC, Bray K, Caton J, Cochran DL, Drisko CH, Fiorellini JP. Treatment of periodontitis by local administration of minocycline microspheres: a controlled trial. J. Periodontol. 2001; 72:1535–1544. [PubMed: 11759865]
24. Kashi TS, Eskandarion S, Esfandyari-Manesh M, Marashi SM, Samadi N, Fatemi SM, Atyabi F, Eshraghi S, Dinarvand R. Improved drug loading and antibacterial activity of minocycline-loaded PLGA nanoparticles prepared by solid/oil/water ion pairing method. Int. J. Nanomed. 2012; 7:221–234.
25. Martin C, Winet H, Bao JY. Acidity near eroding polylactide-polyglycolide in vitro and in vivo in rabbit tibial bone chambers. Biomaterials. 1996; 17:2373–2380. [PubMed: 8982478]
26. Agrawal CM, Athanasiou KA. Technique to control pH in vicinity of biodegrading PLA-PGA implants. J. Biomed. Mater. Res. 1997; 38:105–114. [PubMed: 9178737]
27. Lambs L, Brion M, Berthon G. Metal ion-tetracycline interactions in biological fluids. Part 3. Formation of mixed-metal ternary complexes of tetracycline, oxytetracycline, doxycycline and minocycline with calcium and magnesium, and their involvement in the bioavailability of these antibiotics in blood plasma. Agents Actions. 1984; 14:743–750. [PubMed: 6475671]
28. Joshi Y, Kwak JC. The binding of divalent metal ions to polyelectrolytes in mixed counterion systems: II. Dextransulfate-Mg2+ and dextransulfate-Ca2+ in solutions containing added NaCl or KCl. Biophys. Chem. 1981; 13:65–75. [PubMed: 17000160]
29. Zhang Z, Nix CA, Ercan UK, Gerstenhaber JA, Joshi SG, Zhong Y. Calcium Binding-Mediated Sustained Release of Minocycline from Hydrophilic Multilayer Coatings Targeting Infection and Inflammation. PLoS One. 2014; 9:e84360. [PubMed: 24409292]
30. de Kruif CG, Weinbreck F, de Vries R. Complex coacervation of proteins and anionic polysaccharides. Curr. Opin. Colloid Interface Sci. 2004; 9:340–349.
31. Drogoz A, David L, Rochas C, Domard A, Delair T. Polyelectrolyte complexes from polysaccharides: formation and stoichiometry monitoring. Langmuir. 2007; 23:10950–10958. [PubMed: 17880248]
32. Joshi SG, Paff M, Friedman G, Fridman G, Fridman A, Brooks AD. Control of methicillin-resistant Staphylococcus aureus in planktonic form and biofilms: a biocidal efficacy study of nonthermal dielectric-barrier discharge plasma. Am. J. Infect. Control. 2010; 38:293–301. [PubMed: 20085853]
33. Tiyaboonchai W, Woiszwillo J, Middaugh CR. Formulation and characterization of amphotericin B–polyethylenimine–dextran sulfate nanoparticles. J. Pharm. Sci. 2001; 90:902–914. [PubMed: 11458338]
34. Caminati G, Focardi C, Gabrielli G, Gambinossi F, Mecheri B, Nocentini M, Puggelli M. Spectroscopic investigation of tetracycline interaction with phospholipid Langmuir–Blodgett films. Mater. Sci. Eng. C. 2002; 22:301–305.
35. Nilges MJ, Enochs WS, Swartz HM. Identification and characterization of a tetracycline semiquinone formed during the oxidation of minocycline. J. Org. Chem. 1991; 56:5623–5630.
36. Cornwell DG, Kruger FA. Molecular complexes in the isolation and characterization of plasma lipoproteins. J. Lipid Res. 1961; 2:110–134. [PubMed: 13695618]
37. Orti V, Audran M, Gibert P, Bougard G, Bressolle F. High-performance liquid chromatographic assay for minocycline in human plasma and parotid saliva. J. Chromatogr. B Biomed. Sci. Appl. 2000; 738:357–365. [PubMed: 10718653]
38. Parolo M, Avena M, Pettinari G, Zajonkovsky I, Valles J, Baschini M. Antimicrobial properties of tetracycline and minocycline-montmorillonites. Appl. Clay Sci. 2010; 49:194–199.

39. Gupta D, Tator CH, Shoichet MS. Fast-gelling injectable blend of hyaluronan and methylcellulose for intrathecal, localized delivery to the injured spinal cord. Biomaterials. 2006; 27:2370–2379. [PubMed: 16325904]
40. Jimenez Hamann MC, Tator CH, Shoichet MS. Injectable intrathecal delivery system for localized administration of EGF and FGF-2 to the injured rat spinal cord. Exp. Neurol. 2005; 194:106–119. [PubMed: 15899248]
41. Jimenez Hamann MC, Tsai EC, Tator CH, Shoichet MS. Novel intrathecal delivery system for treatment of spinal cord injury. Exp. Neurol. 2003; 182:300–309. [PubMed: 12895441]
42. Shoichet, MS.; Tate, CC.; Baumann, DM.; LaPlaca, MC. Indwelling Neural Implants: Strategies for Contending with the In Vivo Environment. Reichert, WM., editor. Boca Raton, FL: CRC Press; p. 227-9.
43. Greenblatt D. Reduced serum albumin concentration in the elderly: a report from the Boston Collaborative Drug Surveillance Program. J. Am. Geriatr. Soc. 1979; 27:20–22. [PubMed: 759470]
44. Felgenhauer K. Protein size and cerebrospinal fluid composition. Klin. Wochenschr. 1974; 52:1158–1164. [PubMed: 4456012]
45. Menkin V, Warner CR. Studies on Inflammation: XIII. Carbohydrate Metabolism, Local Acidosis, and the Cytological Picture in Inflammation. Am. J. Pathol. 1937; 13:25–244. 1. [PubMed: 19970311]
46. Gupta AK, Zygun DA, Johnston AJ, Steiner LA, Al-Rawi PG, Chatfield D, Shepherd E, Kirkpatrick PJ, Hutchinson PJ, Menon DK. Extracellular Brain pH and Outcome following Severe Traumatic Brain Injury. J. Neurotrauma. 2004; 21:678–684. [PubMed: 15253796]
47. Pautke C, Otto S, Reu S, Kolk A, Ehrenfeld M, Sturzenbaum S, Wolff KD. Bisphosphonate related osteonecrosis of the jaw--manifestation in a microvascular iliac bone flap. Oral Oncol. 2011; 47:425–429. [PubMed: 21478047]
48. Gao ZG, Lee DH, Kim DI, Bae YH. Doxorubicin loaded pH-sensitive micelle targeting acidic extracellular pH of human ovarian A2780 tumor in mice. J. Drug Targetting. 2005; 13:391–397.
49. Wessels J, Ford W, Szymczak W, Schneider S. The complexation of tetracycline and anhydrotetracycline with Mg2+ and Ca2+: A spectroscopic study. J. Phys. Chem. B. 1998; 102:9323–9331.
50. Coleman JW. Nitric oxide in immunity and inflammation. Int. Immunopharmacol. 2001; 1:1397–1406. [PubMed: 11515807]
51. Amin AR, Attur MG, Thakker GD, Patel PD, Vyas PR, Patel RN, Patel IR, Abramson SB. A novel mechanism of action of tetracyclines: effects on nitric oxide synthases. Proc. Natl. Acad. Sci. U. S. A. 1996; 93:14014–14019. [PubMed: 8943052]
52. Chow KT, Chan LW, Heng PW. Formulation of hydrophilic non-aqueous gel: drug stability in different solvents and rheological behavior of gel matrices. Pharm. Res. 2008; 25:207–217. [PubMed: 17909742]
53. Zimmerli W, Sendi P. Pathogenesis of implant-associated infection: the role of the host. Semin. Immunopathol. 2011; 33:295–306. [PubMed: 21603890]
54. Hetrick EM, Schoenfisch MH. Reducing implant-related infections: active release strategies. Chem. Soc. Rev. 2006; 35:780–789. [PubMed: 16936926]
55. Poelstra KA, Barekzi NA, Rediske AM, Felts AG, Slunt JB, Grainger DW. Prophylactic treatment of gram-positive and gram-negative abdominal implant infections using locally delivered polyclonal antibodies. J. Biomed. Mater. Res. 2002; 60:206–215. [PubMed: 11835177]
56. Wu P, Grainger DW. Drug/device combinations for local drug therapies and infection prophylaxis. Biomaterials. 2006; 27:2450–2467. [PubMed: 16337266]
57. Eliopoulos GM, Maragakis LL, Perl TM. Acinetobacter baumannii: epidemiology, antimicrobial resistance, and treatment options. Clin. Infect. Dis. 2008; 46:1254–1263. [PubMed: 18444865]
58. Liu D, Liu J, Sun D, Wen J. The time course of hydroxyl radical formation following spinal cord injury: the possible role of the iron-catalyzed Haber-Weiss reaction. J. Neurotrauma. 2004; 21:805–816. [PubMed: 15253806]
59. Lewen A, Matz P, Chan PH. Free radical pathways in CNS injury. J. Neurotrauma. 2000; 17:871–890. [PubMed: 11063054]

60. Uttara B, Singh AV, Zamboni P, Mahajan RT. Oxidative stress and neurodegenerative diseases: a review of upstream and downstream antioxidant therapeutic options. Curr. Neuropharmacol. 2009; 7:65–74. [PubMed: 19721819]

61. Garcia-Martinez EM, et al. Mitochondria and calcium flux as targets of neuroprotection caused by minocycline in cerebellar granule cells. Biochem. Pharmacol. 2010; 79:239–250. [PubMed: 19682437]

62. Kraus RL, Pasieczny R, Lariosa-Willingham K, Turner MS, Jiang A, Trauger JW. Antioxidant properties of minocycline: neuroprotection in an oxidative stress assay and direct radical-scavenging activity. J. Neurochem. 2005; 94:819–827. [PubMed: 16033424]

63. Pi R, Li W, Lee NT, Chan HH, Pu Y, Chan LN, Sucher NJ, Chang DC, Li M, Han Y. Minocycline prevents glutamate-induced apoptosis of cerebellar granule neurons by differential regulation of p38 and Akt pathways. J. Neurochem. 2004; 91:1219–1230. [PubMed: 15569265]

64. Ek CJ, Habgood MD, Callaway JK, Dennis R, Dziegielewska KM, Johansson PA, Potter A, Wheaton B, Saunders NR. Spatio-temporal progression of grey and white matter damage following contusion injury in rat spinal cord. PLoS One. 2010; 5:e12021. [PubMed: 20711496]

65. Liu XZ, et al. Neuronal and glial apoptosis after traumatic spinal cord injury. J. Neurosci. 1997; 17:5395–5406. [PubMed: 9204923]

66. Wang X, et al. Towards Effective and Safe Thrombolysis and Thromboprophylaxis: Preclinical Testing of a Novel Antibody-Targeted Recombinant Plasminogen Activator Directed Against Activated Platelets. Circ. Res. 2014; 114:1083–1093. [PubMed: 24508759]

67. Moore AH, Bigbee MJ, Boynton GE, Wakeham CM, Rosenheim HM, Staral CJ, Morrissey JL, Hund AK. Non-Steroidal Anti-Inflammatory Drugs in Alzheimer's Disease and Parkinson's Disease: Reconsidering the Role of Neuroinflammation. Pharmaceuticals. 2010; 3:1812–1841.

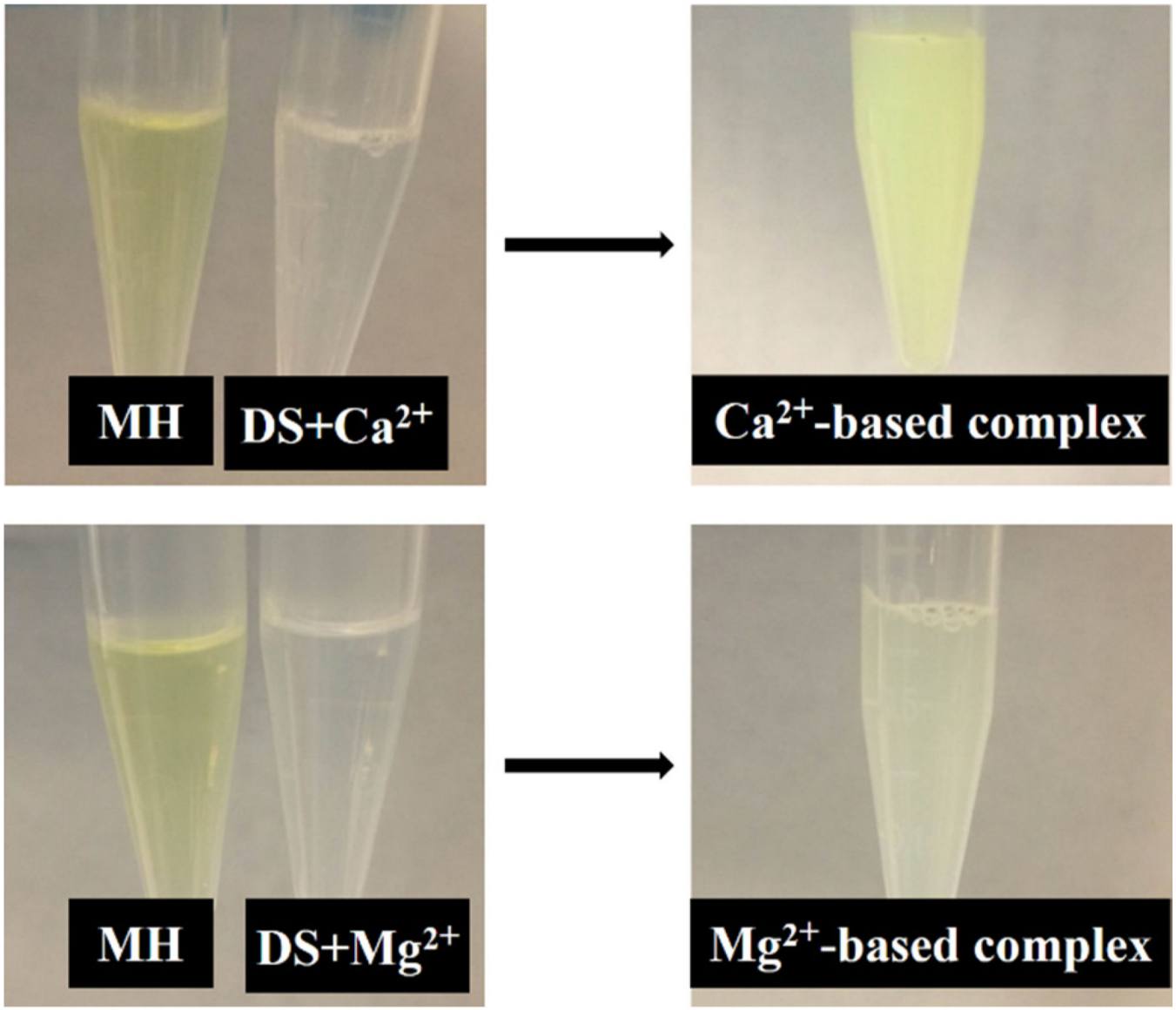

Figure 1.

Macroscopic observation of metal ion-mediated complex coacervation. Addition of Mg^{2+} or Ca^{2+} ions to DS solution does not induce complex formation. When mixing MH, DS and Mg^{2+} or Ca^{2+} solutions together insoluble complexes were formed.

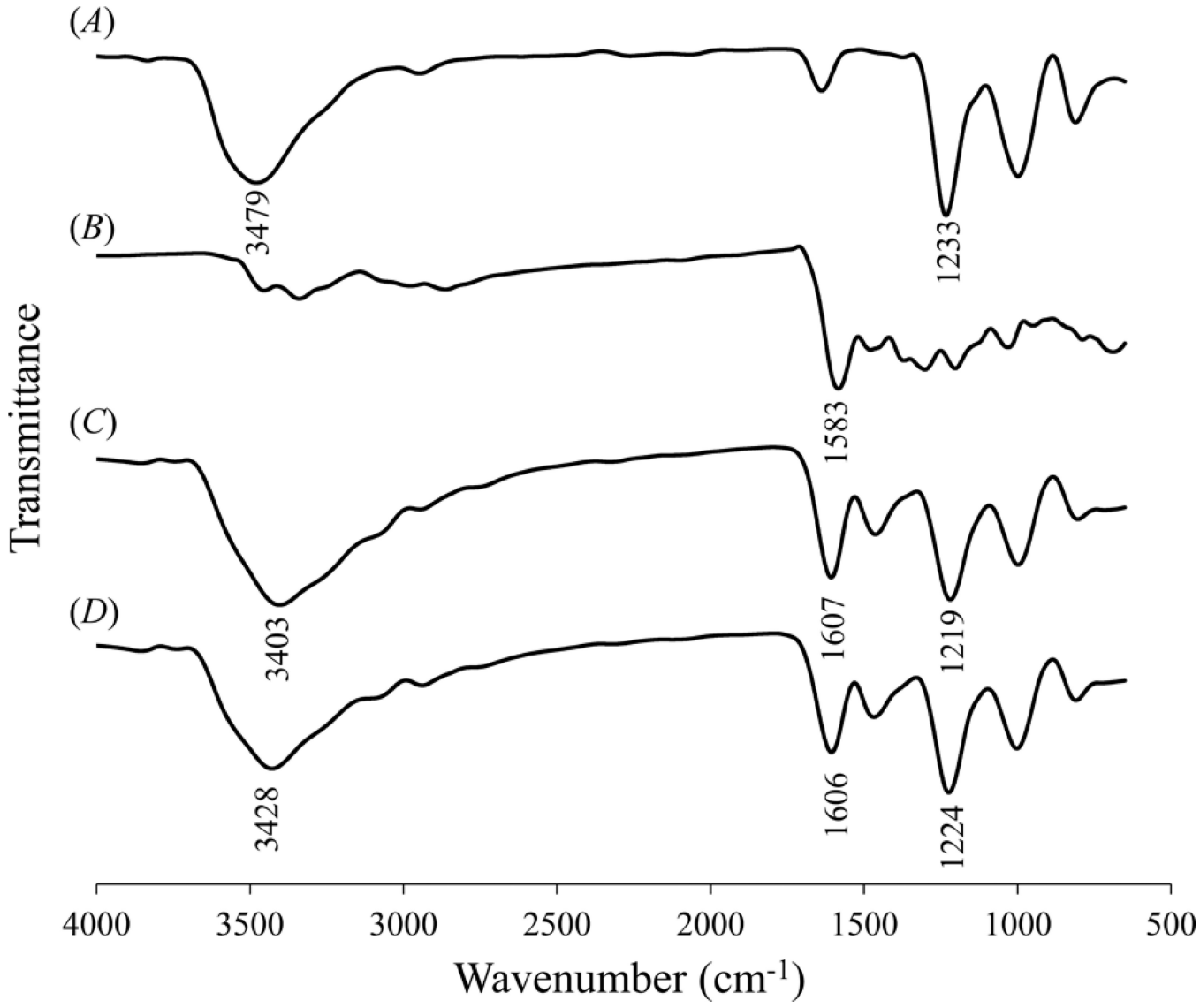

Figure 2.
FTIR spectra of (*A*) DS, (*B*) MH, (*C*) Ca^{2+}-based complex, and (*D*) Mg^{2+}-based complex.

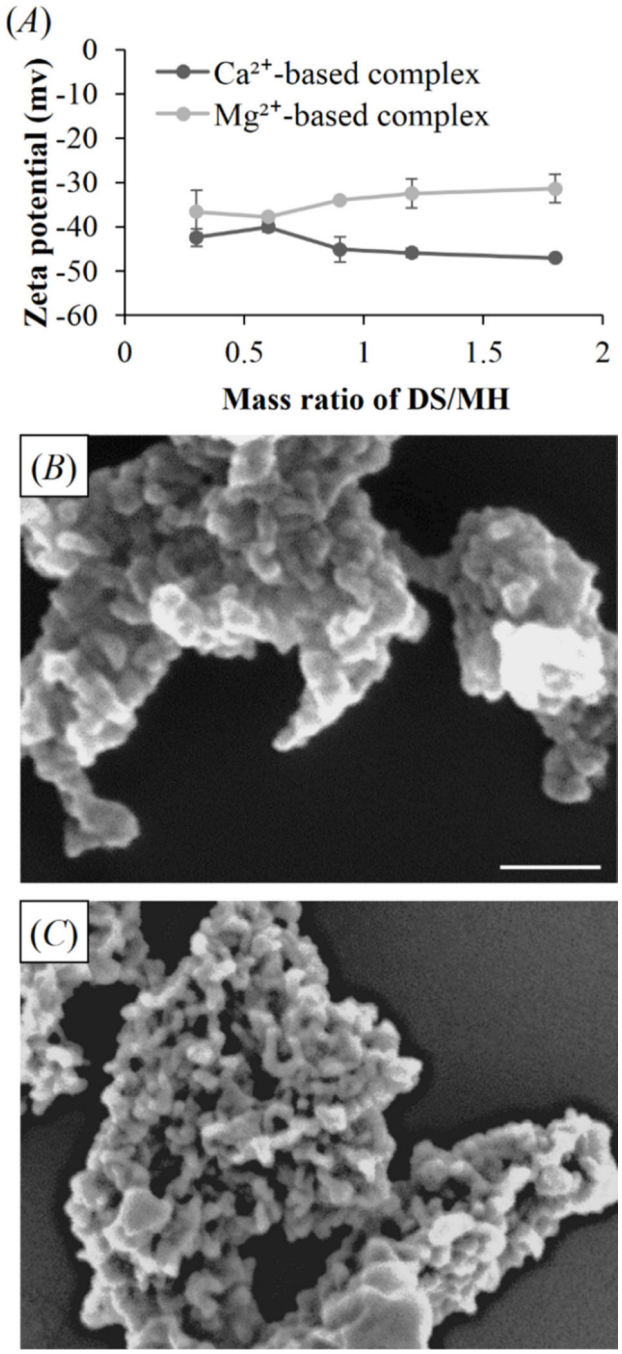

Figure 3.

(*A*) Zeta potential of complexes at different DS/MH ratios. SEM images of (*B*) Ca^{2+}-based complex, and (*C*) Mg^{2+}-based complex. Scale bar = 200 nm.

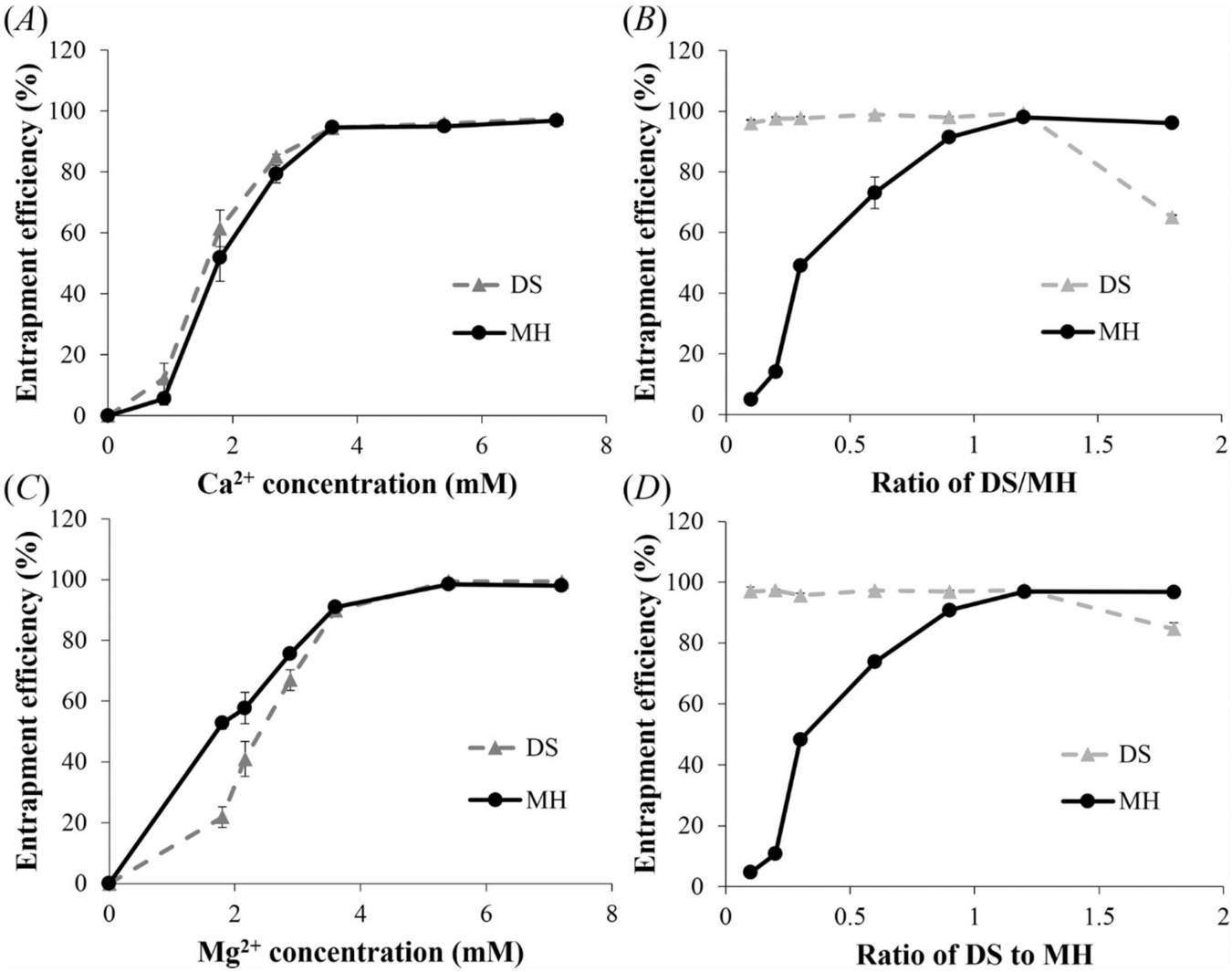

Figure 4.

Effect of metal ion concentration and DS/MH ratio on the entrapment efficiency of DS and MH. (*A*), (*B*) Ca^{2+}-based complex; (*C*), (*D*) Mg^{2+}-based complex. Concentration of DS was 1.2mg/ml in (*A*) and (*C*), while concentration of metal ion (Ca^{2+} or Mg^{2+}) was 7.2mM in (*B*) and (*D*). Data shown are average ± STD (n=3).

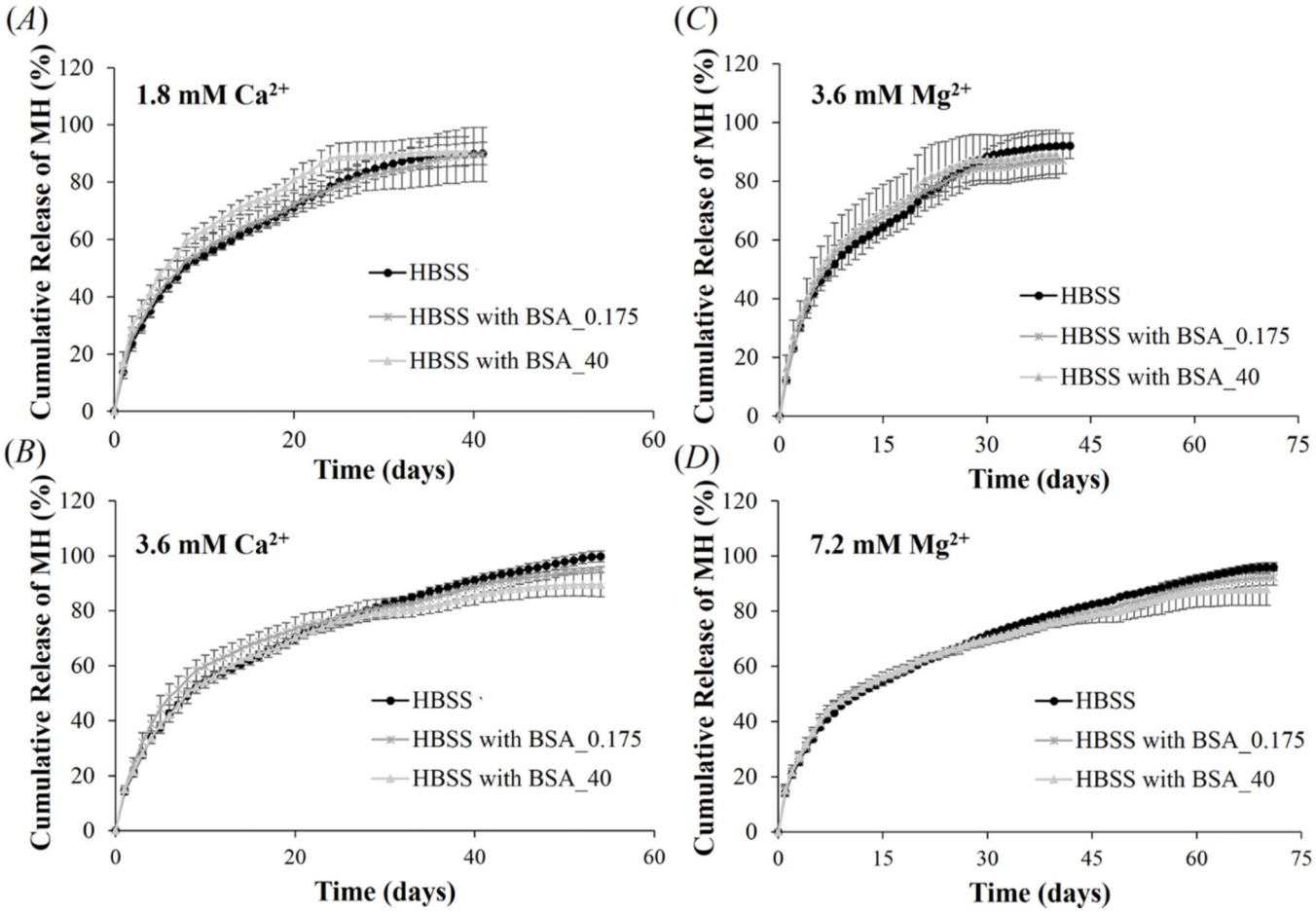

Figure 5.

Effect of Ca^{2+} (*A*) and (*B*), and Mg^{2+} (*C*) and (*D*) concentration on MH release from Ca^{2+}- or Mg^{2+}-based complexes, fabricated by mixing 1.2 mg/ml DS, 1 mg/ml MH, and different concentrations of metal ions. Three different release media were used: HBSS without BSA, HBSS with 0.175 and 40 mg/ml of BSA. Data shown are average ± STD (n=3).

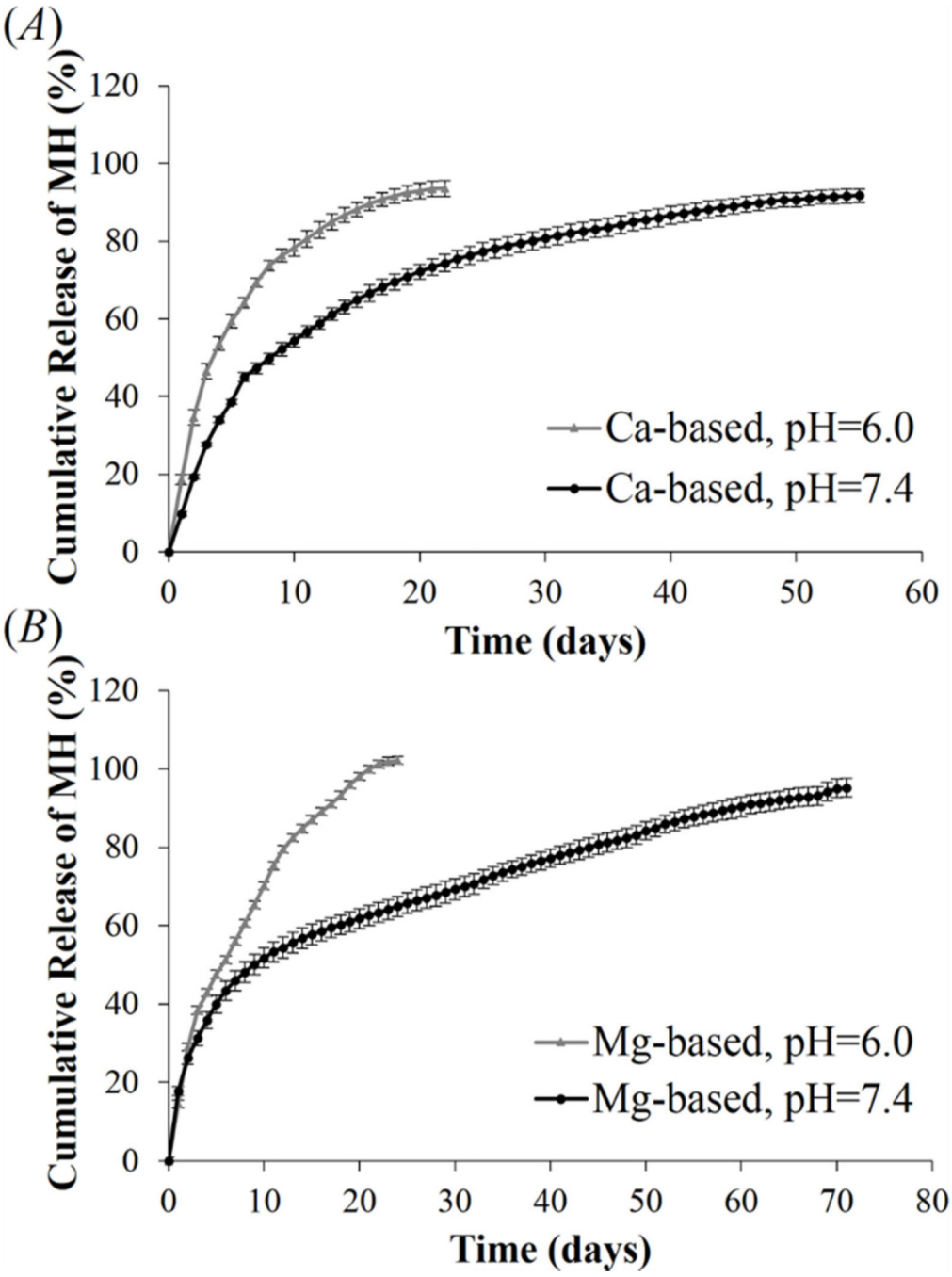

Figure 6.

Effect of pH on MH release from (*A*) Ca^{2+}-based complex, and (*B*) Mg^{2+}-based complex. Complexes were fabricated by mixing 1.2 mg/ml of DS, 1 mg/ml of MH and 7.2 mM metal ions together. Data shown are average ± STD (n=3).

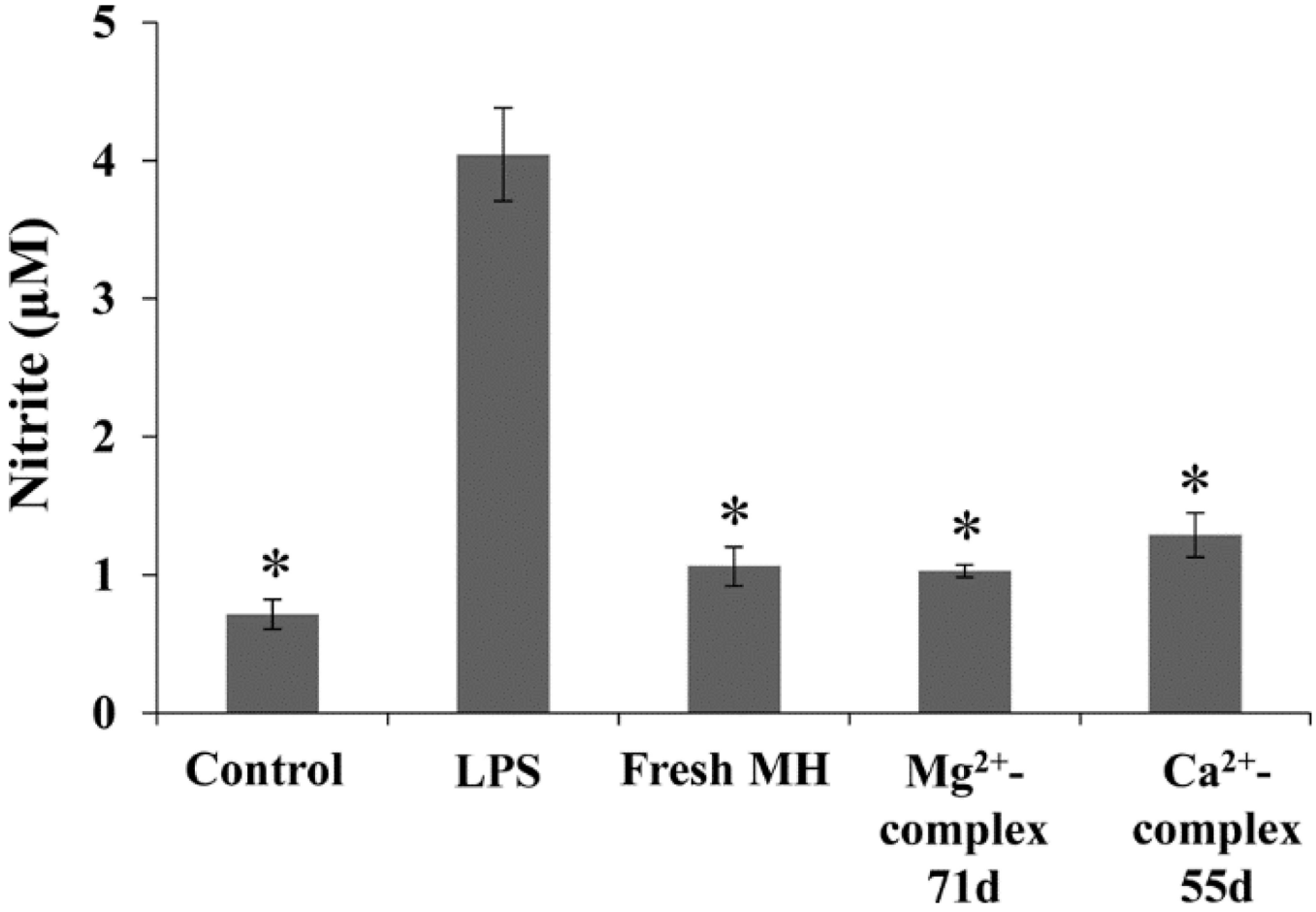

Figure 7.

The anti-inflammatory activity of released MH. NO production by macrophages treated with LPS, LPS and fresh MH, and LPS and MH released from Ca^{2+}- or Mg^{2+}-based complex on day 55 or day 71. Cells without any treatment were used as control. *$P < 0.05$ compared with LPS-treated culture. Data shown are average ± STD (n=3).

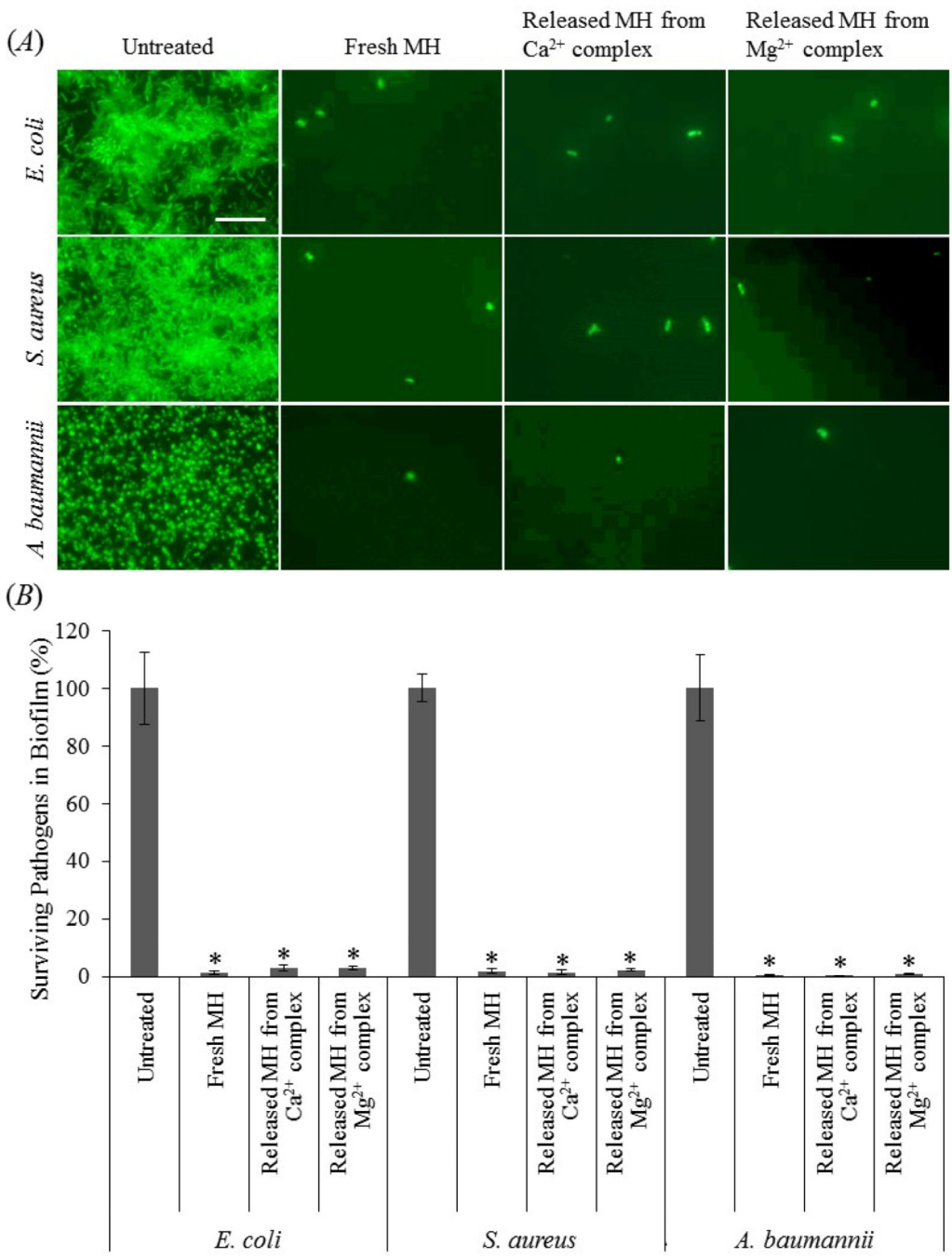

Figure 8.

The anti-biofilm activity of Ca^{2+}- or Mg^{2+}-based complexes. (*A*) Fluorescent images of *E. coli*, *S. aureus*, and *A. baumannii* without any treatment, treated with fresh MH, or MH released from the complexes. The cells were stained with " live" SYTO 9 stain (green fluorescence). Scale bar = 20 μm. (*B*) XTT assay for quantification of surviving bacteria demonstrates significant anti-biofilm activity of fresh MH as well as MH released from the complexes. *, $P < 0.05$ compared with untreated control. Data shown are average ± STD (n=4).

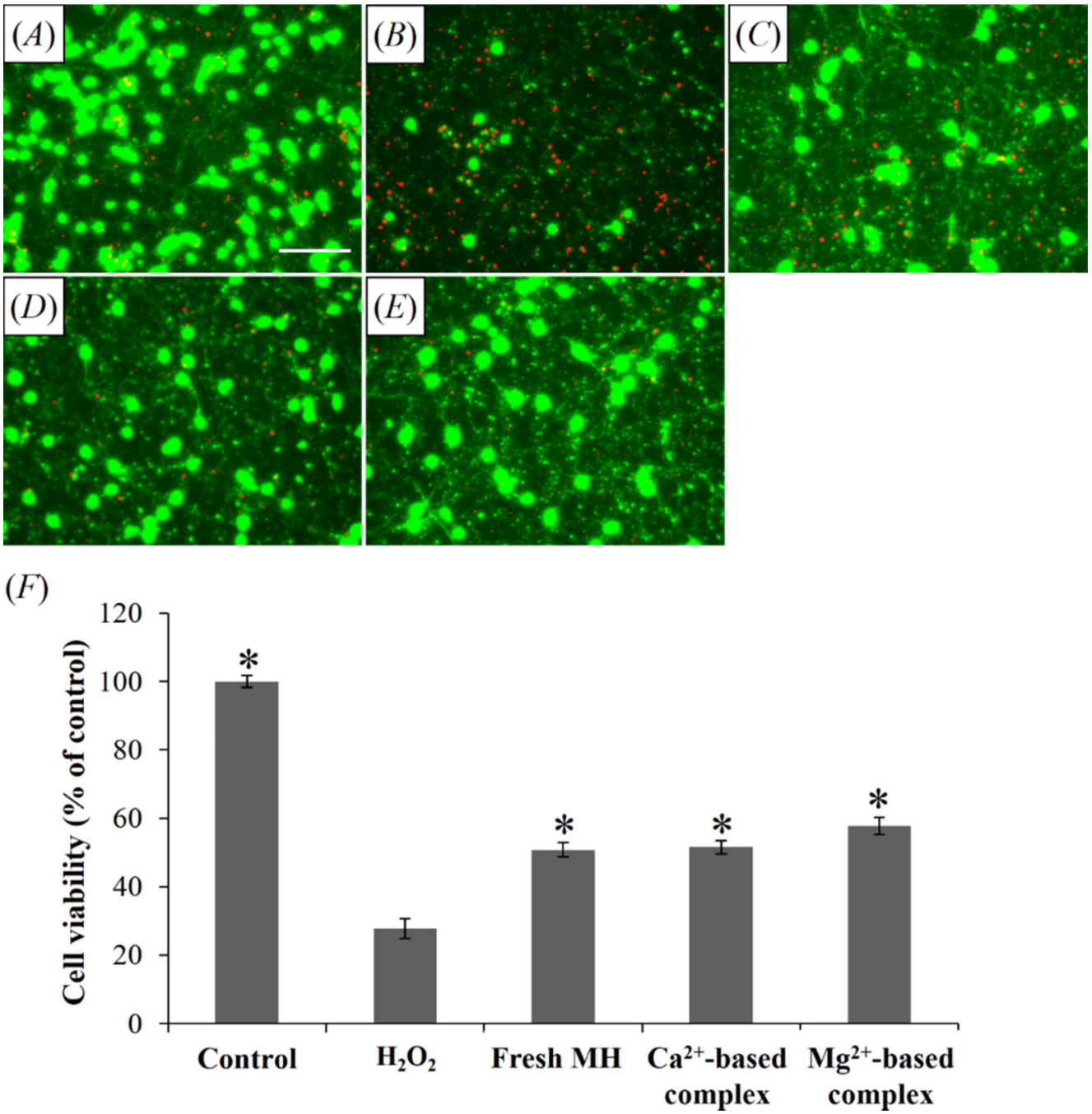

Figure 9.

The neuroprotective activity of released MH. Fluorescent images showing the morphology of cortical neurons (green: "live" cells stained with Calcein AM; red: "dead" cells stained with ethidium homodimer) treated with (*A*) untreated control, (*B*) 100 μM H_2O_2, (*C*) 100 μM H_2O_2 and fresh MH, (*D*) 100 μM H_2O_2 and MH released from Ca^{2+}-based complex, and (*E*) 100 μM H_2O_2 and MH released from Mg^{2+}-based complex. Scale bar = 50 μm. (*F*) Cell viability with different treatments. **P* < 0.05 compared with H_2O_2-treated group. Data shown are average ± STD (n=3).

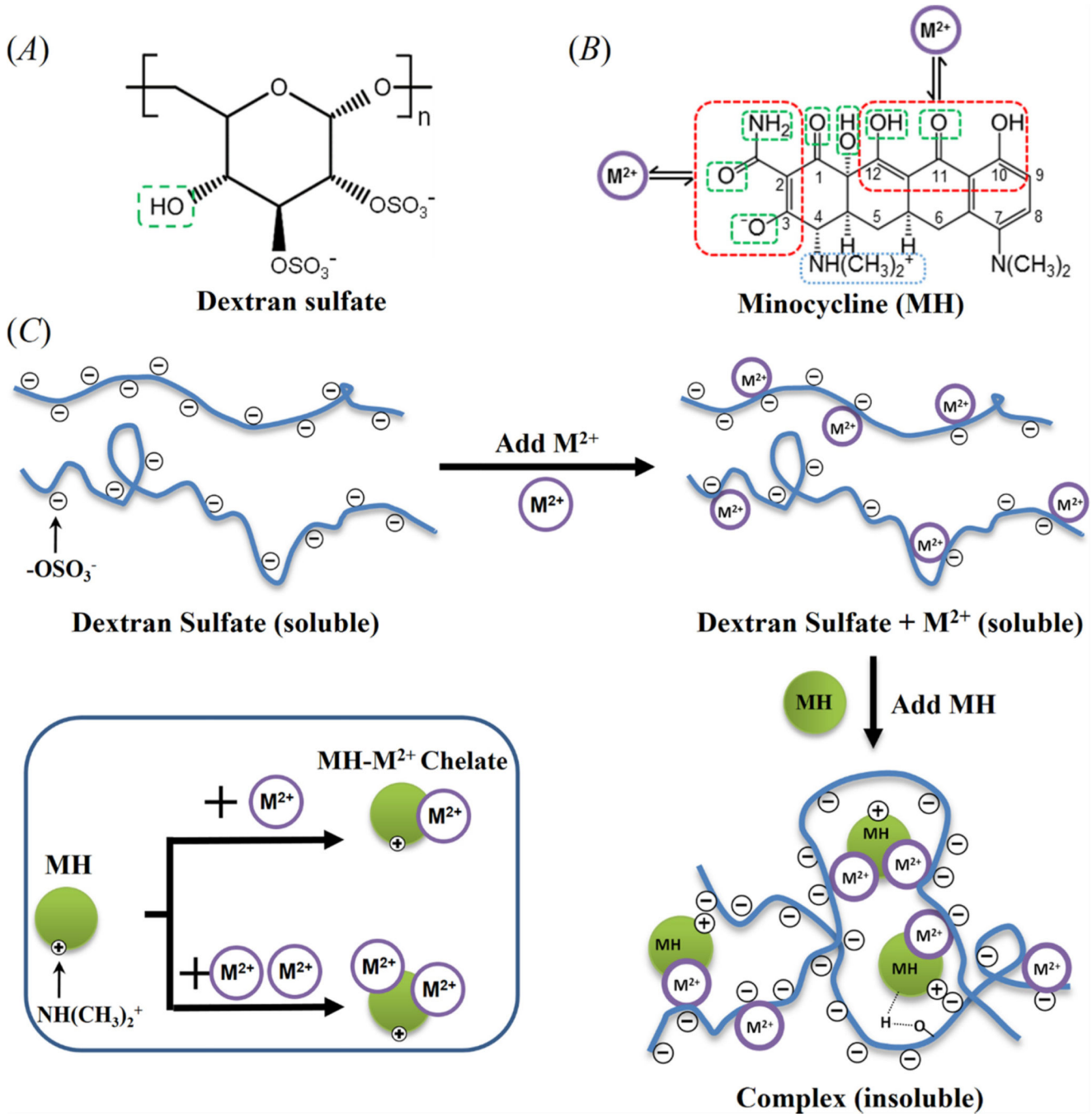

Scheme 1.

Chemical structures of (*A*) DS, and (*B*) MH. The Green boxes mark the chemical groups that can participate in hydrogen bonding, red boxes mark the metal ion chelating sites in MH, and the blue box marks the positively charged ammonium group in MH which can potentially participate in the electrostatic interaction with DS. (*C*) Schematic of complex formation. One MH molecule can bind to two or more chemical groups in DS simultaneously through metal ion binding, hydrogen bonding, and electrostatic interactions

to induce intra and intermolecular crosslinking of DS molecules which leads to insoluble complex formation. M^{2+} denotes metal ions.